EXPERIMENTAL VALIDATION OF OPTICAL SIMULATION FOR COMPLEX BUILDING INTEGRATED PHOTOVOLTAIC SYSTEM

Nebojša Jakica[1], Alessandra Zanelli[1], Francesco Frontini[2]
1 Department of Architecture, Built Environment and Construction Engineering
Politecnico di Milano, Via Bonardi 9, 20133 Milan, Italy
nebojsa.jakica@polimi.it
alessandra.zanelli@polimi.it
2 University of Applied Sciences and Arts of Southern Switzerland (SUPSI) Department for Environment Construction and Design (DACD) Institute for Applied Sustainability to the Built Environment (ISAAC)
francesco.frontini@supsi.ch

ABSTRACT: Simulation of BIPV system performance is usually based on a Plane-Of-Array method, adopted from classical PV plant systems, to estimate power generation. This methods is very limited for simulating facades in complex urban environments, such as dense urban areas, as it uses simplified near-field shading to estimate system losses. Furthermore, this approach accounts only for PV electricity yield generation, while neglecting other architectural criteria like daylighting, especially important in case of semi transparent PV facade. For the purposes of complex BIPV facades, other methods, such as ray tracing, are more preferable. Therefore, this research aims to estimate capabilities and accuracy of RADIANCE ray tracing engine to calculate daylighting and irradiance on PV surface. Validation procedure has been carried out for complex BIPV façade module, composed of complex profiled glass tile and semi-transparent Dye-Sensitized Solar Cells. Results showed reasonably good agreement between simulation and experimental measurements, which proves that method is capable for being used for the general purposes of complex BIPV systems.
Keywords: Ray Tracing, Simulation, Dye-Sensitized, Optical Properties, Experimental Methods

1 INTRODUCTION

RADIANCE ray tracing engine is well known for the application in daylighting simulations for decades. Yet, areas such as Complex Fenestration System (CFS) still represent challenging task and range of research have been done so far [1] [2] to develop strategies for assessing their light deflecting properties. While most of the research target particularly field of daylighting, only some multidisciplinary research explored co-simulation methods for complex BIPV systems. One example with opaque thin-film photovoltaics used RADIANCE as a core simulation engine to determine Bidirectional Scattering Function of the module for thermal and daylighting [3] and electricity yield modelling [4]. Moreover, examples such as [5] demonstrated principles of the optical simulation for semi-transparent BIPV systems. This paper, however, aims to unify some parts of these methods and validate optical simulation, concerning both daylighting and irradiation on PV, for the complex TIFAN BIPV façade. This façade is made for the purposes of TIFAIN project that aims to demonstrate and explore innovative BIPV concepts by integrating CFS glass prismatic component and semi-transparent Dye-Sensitized Solar Cells. Moreover, project puts a particular focus on architectural innovation of BIPV, concerning design, façade technology, simulation and building performance.

2 VALIDATION METHODOLOGY

Validation methodology is based on a comparison of optical properties of different BIPV module samples and covers different scales, ranging from material characterization up to daylighting simulation on the architectural building scale level. It composes of two parallel processes: simulation and experimental testing, producing the results that are compared at the end of the process. A graph showing step-by-step methodology process is shown on **Figure 1**. The steps are marked with the symbol steps and grouped into 5 sub-processes. In order to assure result accuracy, environmental conditions and testing were performed three times for the three different sun positions. Methodology ends up with the results comparison from all three tests for the two processes, simulation and experimental testing.

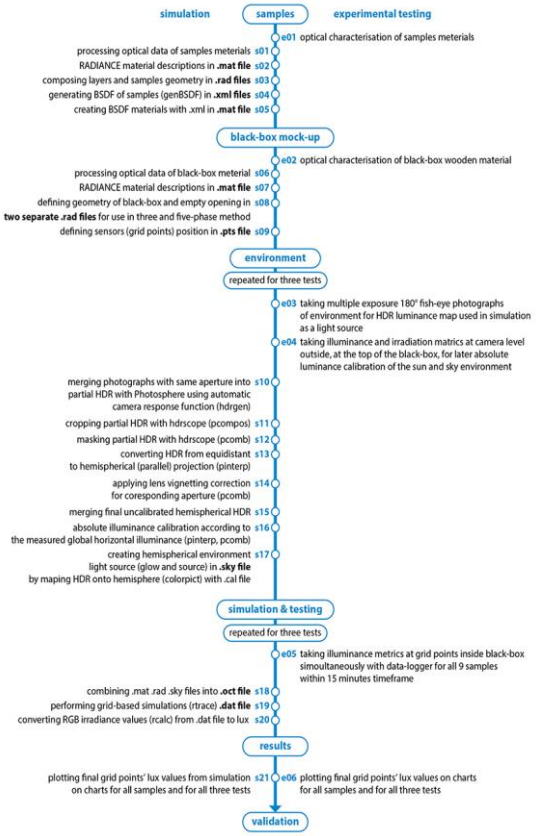

Figure 1: Simulation validation methodology

BIPV samples used in this process are based on one of the two different complex profiled glass tiles. TIFAIN 1 tiles have dimensions of 10x10cm, while TIFAIN 2 tiles are 25x35cm. They have been used as substrate materials for DSSC, which are later encapsulated by EVA foil and placed on clear back sheet glass with the dimensions of 25x105cm. Samples were chosen in the way they cover different level of complexity, ranging from a simple float glass and goes through laminated samples of both TIFAIN 1 and 2 tiles without DSSC, then with half of the grooves surface covered in DSSC and black opaque paint, and finally ends up with a complex BIPV component for both types. All these samples are tested against empty opening and opaque sample for the purposes of calibration and estimating error caused by light leaking through small fissures in the black box.

3 OPTICAL CHARACTERIZATION OF SAMPLES

The first phase of the validation process starts from the optical characterization of materials used in testing module samples: crystal glass substrate material LUXION, EVA encapsulating foil, DSSC and back-sheet supporting glass – **code e01**. Optical properties of these materials are obtained from Optics database, except in the case of LUXION crystal glass and DSSC, where partners from the TIFAIN project had provided optical data (Royal Cristal Rock glass manufacturer for glass and Istituto Italiano di Technologia for DSSC). As RADIANCE simulation is not fully spectrally selective, spectral data for transmittance are integrated over the Red, Green and Blue part of the visible light spectrum to match the requested RADIANCE input for dielectric material – **step s01**. Another input required for the material definition is index of refraction, represented as a single value. Next – **step s02** predicted defining detailed parameters and materials definitions for RADIANCE simulation. These materials are represented as layers that compose samples used in validation process. Since RADIANCE do not support layered materials, each layer is defined as separate geometry with infinitely small distance in between. Geometry and layer descriptions with applied materials for all 8 sample cases were stored in the separate .rad files to be used in the next step – **step s03** and shown on **Figure 2**. Finally, open-source RADIANCE tool genBSDF was used to create BSDF description of the CFS in the WINDOW 6 XML file format – **step s04 - Figure 3**. Final step in material characterization of samples ends with creating material descriptions in .mat file referencing .xml files from the previous step – **step s05**.

4 BLACK-BOX MOCK-UP

For the purposes of the project TIFAIN, full-scale mock-up was constructed in Cantu, Italy, where experimental testing took place. Full-scale mock-up offered many benefits comparing to the scaled mock-up, as for example issues and errors that can appear in a procedure with scaled models [2]. TIFAIN mock-up was built as a cubic box with the dimensions of 3m x 1,05m x 3m representing full 3m height of a typical office room with the 3m depth to get enough variation in the daylighting levels from façade plane inwards. However, for the process of validation all lateral sides were in closed position and only one opening of 1,05m x 0,25m on the top was used as a base for placing all samples. Schematic view of the mock-up geometry and sensors' locations are presented in **Figure 4**.

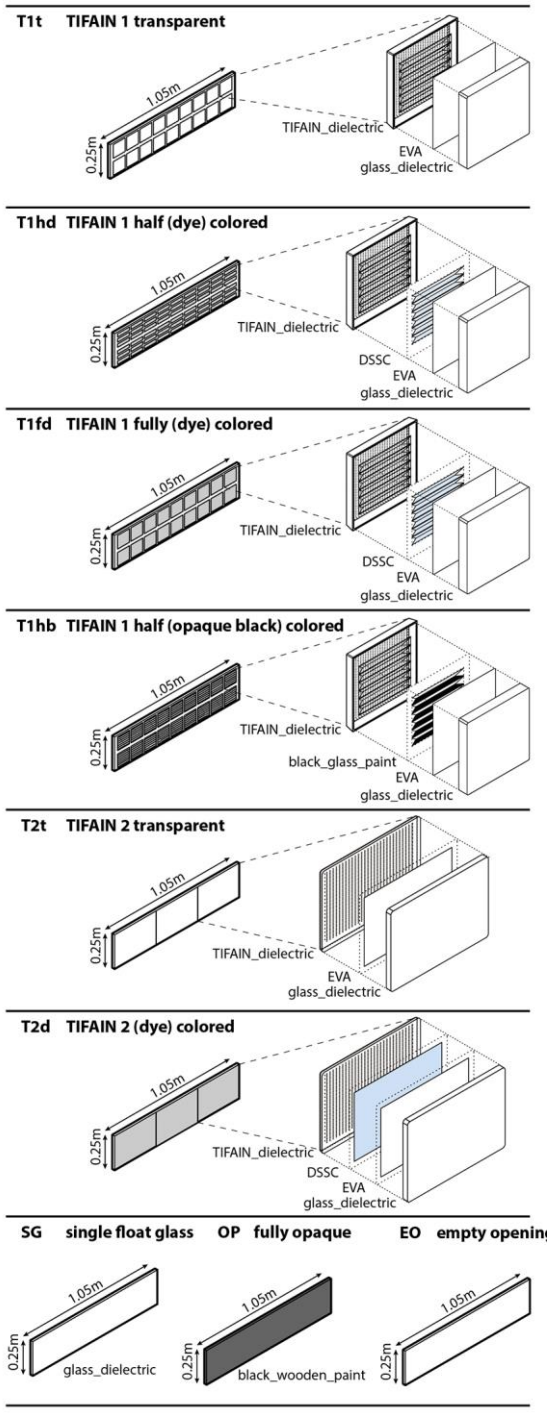

Figure 2: Layer composition of the samples

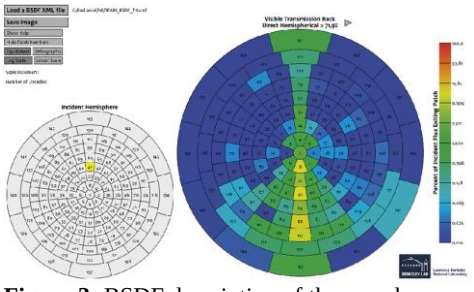

Figure 3: BSDF description of the samples

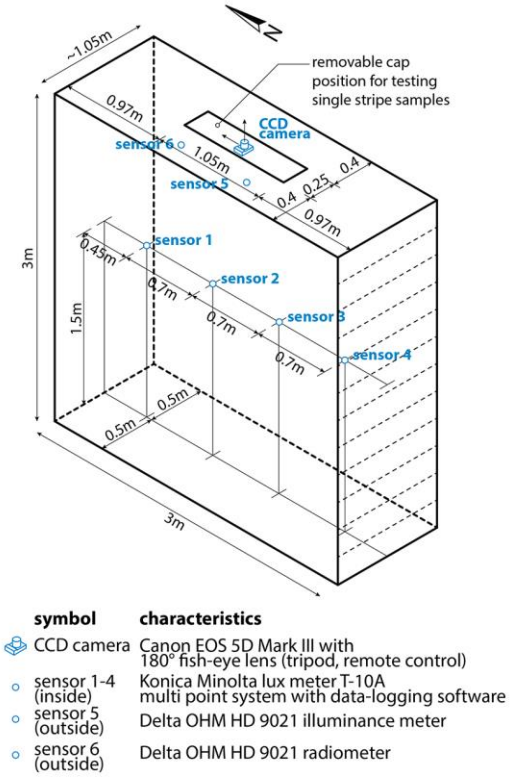

Figure 4: Mock-up geometry and sensors' locations

Whole mock-up was built with two materials, plywood panels painted in black and steel supporting structure on the outer side. This allowed facilitating of the validation procedure as only one material had to be optically characterized – **step e02**. Standard black mate painted plywood material was defined as a RADIANCE material – **step s06, s07**. Geometry of the black-box was defined in Rhinoceros 3D and converted into .rad file with the Honeybee plugin for Grasshopper [6] based on RADIANCE – **step s08**. Honeybee was also used to define sensor points and automatically write their description in .pts file from 3d location and orientation in Rhinoceros 3D – **step s09**. Images of the mock-up and samples are shown on **Figure 5**.

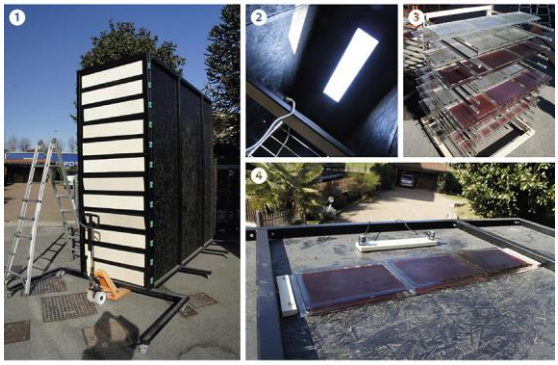

Figure 5: (1) black-box mock-up exterior view (2) empty opening interior view (3) samples (4) one sample placed on empty opening

5 ENVIRONMENT

5.1 Experimental measurements and equipment

Measurements used for the validation process can be grouped in three types. First type relates to capturing environmental condition of the sun, sky and surroundings in form of full hemispherical luminance distribution map that can be used in simulation process to reproduce the same luminance environment as it was during the experimental testing. For this validation, largely available equipment in form of full-frame CCD camera with 180° fish-eye lens and tripod, were used to create images that are later processed to create High-Dynamic Range Images (HDRI). These 32bit images enabled storing full range of luminance values per each pixel and they were used as a single light source in image-based simulation in RADIANCE – **step e03**. To be able to capture environmental conditions from the point of samples, camera was placed at the same plane as samples, facing upwards, with the top of the camera turned towards north. Experimental testing was repeated three times during two sunny winter days. Variation in sun direction and intensity is provided by taking measurements during early morning, mid-day and late afternoon.

Second type of measuring equipment, sensors 5 and 6 (**Figure 4**), are used for calibration purposes of HRDI. These two sensors, illuminance (lux) meter and radiometer, were attached to the same body remotely with a cable connection. This allowed minimum interference while taking measurements. Sensor nodes were positioned at the camera level, faced upwards as well, to measure global horizontal illuminance and irradiance – **step e04**. These values allowed calibration of the HDRIs explained in – **step s16**.

Last instrument type served for measuring illuminance values at the 4 grid points indoor is presented as a series of four sensors 1-4 in **Figure 4**. This multi-point system of four illuminance meters (inside) facing upwards, was connected by a LAN cable to the main body (outside). Main body was connected with the portable computer that had installed data-logger software to simultaneously take measurements from all sensors at once.

5.2 Capturing Luminance Sky Map – HDRI

Accurate representation of luminance values on HDR images represents challenging task for the CCD camera system. There have been numerous trials to validate RADIANCE light simulation under the standard CIE sky models [7]. These sky models (CIE overcast sky, uniform sky, etc.) can introduce important errors, because these models cannot completely describe environmental conditions on the specific site, especially if surrounded with some buildings like in this case. On the other hand, validations under real sky luminance distribution have also been performed and measured by a professional sky luminance mapping instrument [8]. However, with the development of relatively cheep solutions, comparing to sky scanners, in form of digital cameras, taking sky luminance distribution have been revised. Some papers presented various strategies for dealing with the HDR images for the RADIANCE IBL technique [9]. Each of them showed generally good accuracy, which is greater comparing to the simulations under standard generic sky models created by RADIANCE. Stumpfel et al. [10] suggested that combining images with two apertures of f4 and f16 solves issues of capturing full dynamic range of the direct sun and sky. This research uses this method in order to reach higher accuracy of chosen simulation method in predicting the performance of a complex BIPV system.

Process starts with taking multiple exposure 180° fish-eye photographs recorded in 8bit JPEG format with apertures set to f4 and f16 – **step e03**. **Figure 6** depict these image series. For the visual clarity, images are cropped. At the same time, sensors 5 and 6 on top of the black-box measures global illuminance and radiation at camera level – **step e04**.

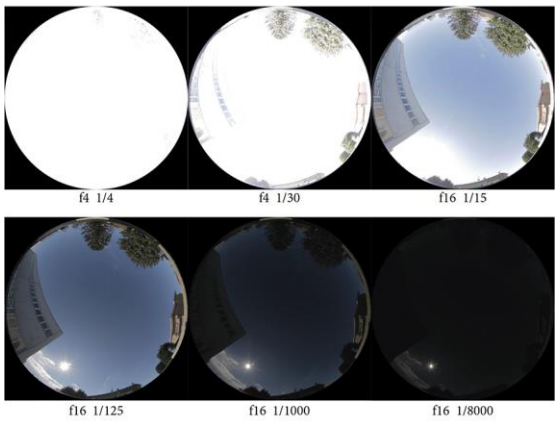

Figure 6: Multiple exposure photographs

Timeframe of the whole process of the sample change took approximately 15 minutes, meaning that each sample took about a minute to be replaced. During this period, no significant change in the sky distribution nor sun position was made that could have potentially influenced results. However, illuminance and radiance measurements were taken at the sensors 5 and 6 at the beginning and at the end of the tests. Difference of the values varied from 2 to 4%, with the greater values associated with the lower sun position. Values are averaged for each test and end value was used for the calibration in the – **step s16**.

The next step in the process takes these series of image and creates HDRI image out of each series – **step s10**. For combining 8bit images into 32bit floating point HDR image, Photosphere software was used. The following four steps: cropping - **step s11**, masking - **step s12**, converting fish-eye image from equidistant to hemispherical projection - **step s13** (**Figure 7**) and applying lens vignetting - **step s14 (Figure 8)**, were conducted in software hdrscope [11]. This software represents GUI for some RADIANCE commands related to image processing, including HDR.

Before proceeding further, it was necessary to map the optical behavior of illuminance meters with the camera one. This conversion - **step s13**, is needed as illuminance meters are hemispherical sensing systems and their optics employs cosine correction. On the other hand, most fish eye lenses perform a geometrical projection where CCD camera takes image through an equidistant projection of light on the lens, which is suitable for being viewed in 2D. In these projections, areas on the edge are distorted to show equal distance through the image from center to the edges **Figure 7**(1). However, since this does not reflect the true spatial image information as captured by the illuminance meter, this projection has to be converted to hemispherical. In other words, to create HDR images that have luminance distribution with the correct values according to the angle of incidence on sensor **Figure 7**(2).

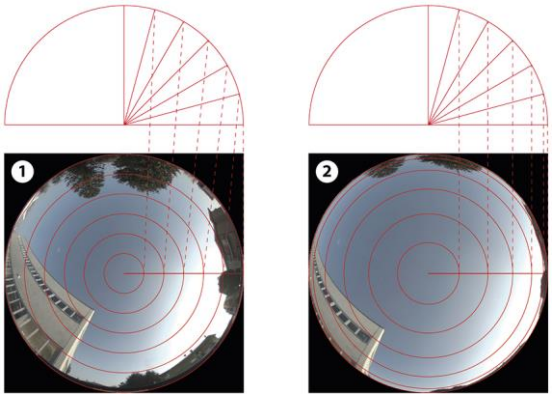

Figure 7: Converting projection mapping (1) equidistant projection (2) hemispherical (parallel) projection

The last step in preparing partial HDRI for being merged into final is lens vignetting correction – **step s14**. Lens Vignetting is a phenomenon that appears due to lens optical and mechanical deviations. Vignetting is represented as a radial non-linear light intensity fall off across the lens. In the peripheral areas of these lenses the luminance values captured by the digital camera image sensor is lower than what appears in the real world, which cause these areas looks darker. This is especially visible with the wider apertures (<8). Therefore, before merging to HDRI, all images has to go through the process of lens vignetting correction to assign vignetting correction mask according to the aperture. Three different vignetting masks are used for each of the three apertures - **Figure 8**. These images show the intensity of the light as a relative measure of luminance values in falsecolor representation for different apertures. Values closer to 1 (in yellow) denote pixels that require no luminance alteration while other colors require proportional luminance correction. These masks are obtained from the camera and lens manufacturer, by specifying camera and lens model.

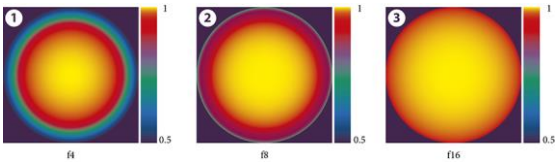

Figure 8: Vignetting correction (1) vignetting mask for aperture f4 (2) vignetting mask for aperture f8 (3) vignetting mask for aperture f16

Finally, partial HDRIs were merged into single HDRIs, again with the Photosphere – **step s15**. Process continues with the absolute illuminance calibration – **step s16**, in order to ensure that the HDR images maintain absolute accuracy. This process requires a calibration factor that should be applied to the images. Calibration factor value is calculated automatically from the global horizontal illuminance measured at the camera level from the sensor 5 and measured illuminance quantity derived from a fisheye photograph.

Process of describing environmental conditions during the tests concludes with the creation of the hemispherical environment light source – **step s17**, in .sky file that includes reference to the final calibrated HDR image and angular.cal file that maps this image to hemispherical environment in RADIANCE.

6 SIMULATION AND EXPERIMENTAL TESTING PROCESS

Simulation and field testing ends with obtaining results in form of illuminance values in lux on predefined positions of the sensors inside the black-box. During this final process all the samples were set to the top position of the mock-up and illuminance metrics were taken for each sample – **step e05**. The same process is repeated virtually based on the previous collected and processed data and files described through the steps s01-s17 and e01-e04.

Process of simulation started with combining files from steps s02, s05, s07, and s17 into an octafile – **step s18**. This form of file is used by RADIANCE to divide the space in boxes containing geometry and performs ray-tracing only in these areas, which speeds up calculation time. Next step presents grid-point simulation – **step s19**, performed with the RADIANCE rtrace function using previously made .oct file and points from step s09. As RADIANCE by default calculates radiometric values for RGB channels separately, last step consists of converting and integrating these values into lux to be able to compare with the field values – **step s20**. This is also the last step of the simulation process that had produced results used in the validation process.

7 EXPERIMENTAL VALIDATION

Main objective of the result validation is to compare accuracy of the simulation and ability to simulate real light behavior through the semi-transparent complex BIPV. Three tests should have ensured enough variability to validate differences of the results, although it would be ideal to repeat the test during different sky condition-overcast, intermediate. However, this was not possible within the timeframe and resources of this research and TIFAIN project. Despite this limitation, results provided enough variation to prove different light deflection from and through samples and therefore light distribution inside the black-box.

All the results were processed and organized into three groups corresponding to the three tests – step s21/e06. Results are presented in **Figure 9**. It can be clearly seen that CFS systems of T1t and T2t showed improved lighting for the tests 2 and test 1 respectively, in comparison to empty opening and simple glazing, that is a consequence of angle optimization for the sun at high altitude. In this case of samples placed horizontally test 1 and test 2 captures this sharp incidence sun angle because sun was either early morning sun (test 2) or late afternoon (test 1). In the third case of test 3, empty opening and simple glazing showed better performance than other samples, as expected. Taking a look onto results of fully colored samples T1fd and T2d, or the samples with transparent PV, in all three test they showed less transmittance of the light, caused by filtration and absorption in the cells, and therefore lower illuminance values. However, this doesn't necessary mean they have lower performance than others. Contrary, this property can be very significant in protecting from the excessive amount of daylighting that can cause glare and discomfort. Furthermore, it means more sun light absorbed in the PV cells and therefore more electricity generated. This can be extremely useful in the areas of the façade near the ceiling suitable for daylighting devices. Other semi-colored samples showed mid-range performances, as they represent balanced mix between transparent and fully colored samples. Differences of the performances are especially visible in the areas of the greater daylighting levels, such as sensors 1 and 2, while sensor 4 collected values very close one to another, often falling within the 10%, which is considered as a common accuracy error of the RADIANCE simulation. Consequently, values of the sensor 1 served as a dominant information for making comparisons and conclusions.

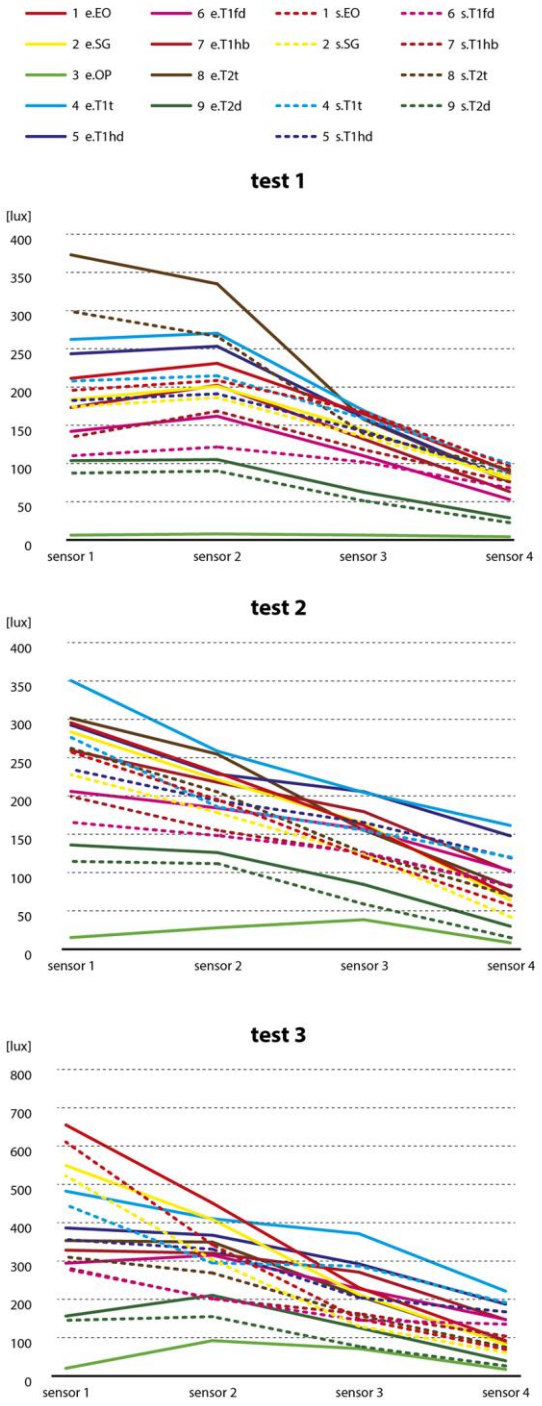

Figure 9: Validation results

In order to estimate potential error, caused by light leaking through the gaps on the shorter lateral side of the black-box, and through the gap between sample on the top and black-box, one opaque sample was used. This is a sample no. 3 OP that appears only in environmental part,

as simulation was designed with absolute precision of the geometry. Illuminance values for this sample are expectedly much lower than other values. These values increases with the amount of sun and they are the greatest in the test 3, under the sun with highest altitude. Nevertheless, these values rises proportionally with the increase of the other values and falls under the 6% of the maximal value, which can be considered as tolerable.

Differences in values appeared due to many different sources, starting from light leaking, material imperfections (CFS, non-homogenous PV disposition, lamination gaps, wooden roughness), inability of CCD camera to capture full dynamic range of the sun and discretization of the sphere in patches in calculation of the BSDF for CFS. Light leaking in form of sample 3. OP is therefore indicator of its contribution to the overall error. These errors become greater with the increase of the direct sunlight, test 3. Errors are more visible in samples containing CFS as RADIANCE used BSDF description of the material to trace rays. As these description is discretized, RADIANCE fails to simulate precisely direct sun through the samples. This is possible with the new five-phase method that calculate direct sun in a separate phase. In this case, thought, it was not possible to use this method in a combination with the Image-based illumination from the field. This method is intended to work only with standard CIE sky models that can be generated with the RADIANCE. Due to this limitation, simulation is performed only as a regular procedure, averaging direct sun in maximum three neighborhood patches. Considering all these potential causes of the error, one to one comparison of the samples show that, with the few exceptions, overall error rarely exceeds 15%.

8 CONCLUSION

Results obtained demonstrate that applied simulation methodology for complex BIPV façade systems is in a general good correlation with the real world measurements under provided sky conditions. Even at some points difference increase, assumption is that these differences are caused by imperfections of the materials and mock-up as well as HDRIs captured. Furthermore, for better assessment of performances under direct sun, higher resolution BSDF is needed. These issues should be eliminated or decreased to a minimal level by introduction of a new five-phase method, and based on the BSDF descriptions of the complex BIPV done in this study. With the computer generated sun and sky and increasing demand in precision, new five-phase method should be capable to deal with these complex BIPV facades.

From the electrical point of view, methodology can be used to predict Quantum Efficiency of such systems more precisely by adopting wavelength spectrum to match one of spectral response PV solar cell and discretizing it into small bands. This should open up new ways of assessing performances for complex BIPV from both architectural side in terms of determining the luminous and solar characteristics of glazing, and possibly from the electrical side in terms of Quantum Efficiency of the PV cells. Putting it into a broader perspective, this should create novel approach of assessing energy and daylight performances and accelerate creation and large-scale implementation of BIPV systems.

9 ACKNOWLEDGEMENTS

This work was supported by the Lombardy Region and the Italian Ministry of Education, Universities and Research (MIUR) under Grant number 30221157 – project TIFAIN - Tessere Integrate di vetro Fotovoltaico per applicazioni Architettoniche INnovative (photovoltaic integrated glass tiles for innovative architectural application - eng.)"

10 REFERENCES

[1] J. de Boer, "Modelling indoor illumination by complex fenestration systems based on bidirectional photometric data," *Energy Build.*, vol. 38, no. 7, pp. 849–868, Jul. 2006.

[2] F. Maamari, M. Andersen, J. de Boer, W. L. Carroll, D. Dumortier, and P. Greenup, "Experimental validation of simulation methods for bi-directional transmission properties at the daylighting performance level," *Energy Build.*, vol. 38, no. 7, pp. 878–889, Jul. 2006.

[3] F. Frontini, "Daylight and solar control in buildings. General evaluation and optimization of a new angle selective glazing façade," Fraunhofer Verlag, Stuttgart, 2011.

[4] W. Sprenger, "Electricity yield simulation of complex BIPV systems," Tu Delft, 2013.

[5] F. José Moralejo–Vázquez, N. Martín–Chivelet, L. Olivieri, and E. Caamaño–Martin, "Optical Characterisation Of Semi-Transparent Pv Modules For Building Integration," in *Proceeding of the 29th EU PVSEC*, Amsterdam, 2014.

[6] M. S. Roudsari, M. Pak, and A. Smith, "Ladybug: A Parametric Environmental Plugin for Grasshopper to Help Designers Create an Environmentally-Conscious Design," in *proceedings of bs2013: 13th conference of international building performance association, chambery, france, august*, 2013, pp. 26–28.

[7] A. McNeil, "A validation of the Radiance three-phase simulation method for modeling annual daylight performance of optically-complex fenestration systems," *J. Build. Perform. Simul. April 2012*, May 2013.

[8] J. Mardaljevic, "Validation of a lighting simulation program under real sky conditions," *Light. Res. Technol.*, vol. 27, no. 4, pp. 181–188, Dec. 1995.

[9] M. Inanici, "Evalution of High Dynamic Range Image-Based Sky Models in Lighting Simulation," *Leukos*, vol. 7, no. 2, pp. 69–84, 2010.

[10] J. Stumpfel, C. Tchou, A. Jones, T. Hawkins, A. Wenger, and P. Debevec, "Direct HDR Capture of the Sun and Sky," in *Proceedings of the 3rd International Conference on Computer Graphics, Virtual Reality, Visualisation and Interaction in Africa*, New York, NY, USA, 2004, pp. 145–149.

[11] V. Kumaragurubaran and M. Inanici, "Hdrscope: high dynamic range image processing toolkit for lighting simulations and analysis," in *Proceedings of the BS2013: 13th Conference of International Building Performance Simulation Association*, 2013, pp. 25–28.